Article

An Improved Approach to Estimate Three-Phase Relative Permeability Functions for Heavy-Oil Displacement Involving Instability and Compositional Effects

Pedram Mahzari * [ID] **, Usman Taura, Alexander J. Cooke and Mehran Sohrabi**

Centre for Enhanced Oil Recovery and CO_2 Solutions, Heriot-Watt University, Edinburgh EH14 4AS, UK; Usman.taura@pet.hw.ac.uk (U.T.); a.cooke@hw.ac.uk (A.J.C.); m.sohrabi@hw.ac.uk (M.S.)
* Correspondence: p.mahzari@hw.ac.uk; Tel: +44-(0)131-451-8094

Abstract: Simultaneous three-phase flow of gas, oil and water is a common phenomenon in enhanced oil recovery techniques such as water-alternating-gas (WAG) injection. Reliable reservoir simulations are required to predict the performance of these injections before field application. However, heavy oil displacement by gas or water can lead to viscous fingering due to the unfavorable mobility ratio between heavy oil and the displacing fluid. In addition, the injection of partially dissolvable gases such as CO_2 can result in compositional effects, which can bring about a significant reduction of oil viscosity and hence can cause variations of the mobility ratio. Estimations of three-phase relative permeability under such conditions are extremely complex, and using conventional techniques for the estimation can lead to erroneous results. We used the results of four coreflood experiments, carried out on a core, to estimate two-phase and three-phase relative permeability. A new history matching methodology for laboratory experiments was used that takes into account the instability and the compositional effects in the estimation processes. The results demonstrate that a simultaneous CO_2 and water injection (CO_2-simultaneous water and gas (SWAG)) can be adequately matched using the relative permeabilities of a secondary gas/liquid and a tertiary oil/water. In heavy oil WAG injection, the injected water follows the CO_2 path due its lower resistance as a result of the CO_2 dissolution in the oil and the resultant reduction of the oil viscosity. This is contrary to WAG injection in conventional oils, where gas and water open up separate saturations paths. It is also important to include capillary pressure (Pc), even in high permeable porous media, as we observed that the inclusion of capillary pressure dampened the propagation of the viscous fingers and hence helped the front to become stabilized, leading to a more realistic simulated sweep efficiency.

Keywords: heavy oil; CO_2 injection; enhanced oil recovery; three phase simulation; viscous fingering; compositional simulation; WAG injection

1. Introduction

Recovery of heavy (viscous) oil by gas or water injection may suffer from viscous fingering: a well-known instability phenomenon in porous media that results from adverse mobility ratio between the displaced fluid (oil) and the displacing fluid (gas or water). The consequence of this phenomenon is the bypassing of a significant amount of oil, which would cause the remaining oil to be divided in two forms, i.e., pore-scale residual oil and bypassed oil. When a one-dimensional (1D) model is used to simulate such displacement, the frontal instability cannot be captured, leading to the lumping of these two forms of remaining oil into one parameter, i.e., the residual oil saturation (*Sor*). Therefore, an unrealistic evaluation of displacements would be obtained when a 1D model is used.

Additionally, a relative permeability obtained from a stable displacement when used in the simulation of an unstable displacement may lead to erroneous result [1,2]. In such a case, an additional dimension would be required in the model to effectively capture the instability occurring in the front.

The effect of viscous fingering on heavy oil recovery by gas and water has been studied extensively at laboratory scales [3–7] and at field scale [8,9]. Despite the predominant impact of the mobility ratio on viscous fingering, the stability of heavy oil displacement by gas can also be affected by capillary pressure, which can lead to an exacerbation or dampening of the viscous fingers [10–15].

To improve the conformance, and consequently the sweep efficiency, of such displacements, several techniques have been investigated, which often involve the simultaneous flow of three or more immiscible fluids, including oil, water and gas. Numerical simulation models are now increasingly being utilized to consolidate our understanding of the displacement patterns, due mainly to the recent enhancement in computer speed and memory. Hence, by employing a typical reservoir simulator, several recovery methods can be evaluated for feasibility and efficiency in order to determine the recovery method that is most efficient in terms economic, practicality and environmental impacts. For the recovery methods involving the simultaneous flow of three fluids, a three-phase relative permeability would be required to simulate the process. Inaccuracies in this important flow function have been identified as one of the major sources of uncertainty in reservoir performance prediction [16].

Three-phase relative permeability has been widely investigated for immiscible gas injections [17,18] and for water alternating gas [19,20]. Two major experimental techniques are available for the estimation of three-phase relative permeability: the steady state and the unsteady state method [21]. In the steady state displacement method, the two phases are injected at a fixed ratio continuously until the saturation in the core and the pressure drop across the sample becomes unchanged; an indication that the system has achieved steady-state. It is difficult to estimate relative permeability curves for heavy oil systems using this method because of the inherent experimental artefacts associated with the method, which is compounded by the high viscosity of the oil. The more common approach is the unsteady-state method, also known as the dynamic displacement method. In this case, the porous media is initially saturated with oil at connate water saturation and then displaced by a second fluid; the produced volume of the injected fluid and the produced volume of oil, as well as the pressure drop across the medium, are then used to calculate the relative permeability curves using analytical techniques that are based on methods developed by Welge [22] and Johnson et al. [23]. These include the Johnson–Bossler–Naumann [23]—commonly known as the JBN—method and the Jones and Roszelle analytical method [24]. Alternatively, history matching techniques can also be used to determine the relative permeability by representing the curves with a parametric equation and matching the production history data parameter [25–29].

Although the importance of reliable experimental data in numerical analysis is well recognized, laboratory measurements of three-phase relative permeability for viscous systems are usually not attempted. The reason for this appears to be the time and expense involved, as well as the poor reliability of available experimental data [18]. Quite often, relative permeability values are estimated from correlations such as Stone I and II models [30,31] and the Baker model [32]. The Stone models make use of the probability model (probabilistic methods) which incorporates two sets of two-phase relative permeability data to predict the relative permeability of the intermediate wet phase in a three-phase system. The Baker model is a simplistic three-phase relative permeability correlation that is based on saturation-weighted interpolation (SWI) between two-phase relative permeability data in which the three-phase relative permeability of each phase in assumed to be a function of two saturations. Relative permeability has also been examined to strongly depend on saturation history in cyclic processes, otherwise known as hysteresis. This phenomenon has been extensively investigated experimentally and numerically [14,19,33–36]. A few three-phase relative permeability models have been proposed which incorporate hysteresis, compositional and interfacial tension (IFT) effects, these include the Jerauld model [37] which attempts to predict three-phase, gas, oil and water hysteresis as well as relative permeability dependence on composition and gas/oil IFT. The Blunt

empirical model [38] also accounts for hysteresis, changes in hydrocarbon composition as well as trapping of gas, oil and water. Nevertheless, in three-phase displacements of viscous oils, the viscous forces would be dominant and hence, there is a need to investigate if the hysteresis (in conventional systems) pertinent to wettability may not be significant in heavy oil displacements. In other words, it can be conceivable that change in gas/oil/water relative permeabilities during WAG injection can be likened to variation of fluid viscosities rather than percolation type of fluid invasion. Also, the use of pore-network modelling, suggested for conventional light oil systems [39], may not be applicable for systems under significant instabilities and bypassing due to violation of percolation theories.

Since all these correlations utilize two-phase relative permeability data as an input in the estimation of three-phase relative permeability, their inaccuracies can be compounded by uncertainty in the two-phase relative permeability data. More so, when the two-phase relative permeability for a heavy oil displacement by gas or water is determined by history matching technique, is it important to ensure that an appropriate model which mimics the instability in the system is utilized. It is therefore important for any numerical studies of heavy oil displacements with unstable fronts to reconstruct the development of the instabilities. The objective of this research is to numerically investigate three-phase relative permeability data in heavy oil systems in which the displacement of the viscous oil was unstable. A series of coreflood experiments, namely CO_2 injections in secondary and tertiary, and water-alternating-gas injection scenarios, were considered for the numerical investigation. Here, it was attempted to demonstrate the necessity of employing a sophisticated method, i.e., 2D high resolution compositional model, for the estimation of relative permeability (if compared to conventional 1D simulation) for cases under unstable displacement and significant compositional interactions. The aim has been to examine the outcome of this new method of simulating laboratory experiments by incorporating the estimated relative permeabilities for forward simulation of a similar experiment. This would indicate that, for the displacement of viscous oils, changes of relative permeability in three-phase, which is conventionally named three-phase WAG hysteresis, would be dominantly controlled by changes in fluid viscosities.

2. Methodology

Our approach of estimating gas, oil and water, and three-phase relative permeability for heavy oil displacement, is based on history matching of the two-phase (gas/oil and oil/water) unsteady state displacement experiments in which instability and mass transfer simultaneously took place. A compositional simulator (CMG-GEM) was utilized to incorporate the fluid flow and compositional effects. The compositional effects need to be implemented due to drastic changes in oil viscosity as CO_2 was dissolved in the resident oil. Figure 1 illustrates the relationship between oil viscosity and CO_2 dissolution. An equation of states (EOS) was tuned to capture the compositional effects based on composition of the oils produced from the coreflood experiment (rather than conventional PVT experiments). Details of the improved methodology for EOS modelling can be found in [2]. A history matching methodology which incorporates instability and compositional effect proposed by [2] was adopted. Using CMG-CMOST (this is CMG software for optimization purposes) with its CMG designed exploration and controlled evolution (CMG's proprietary algorithm) algorithm for minimization of objective functions, a high-resolution two dimensional (2D) compositional model was used to simulate and history match coreflood experiments. This optimization algorithm is based on estimation posterior probability function of a parameter, which is expressed by the following equations:

$$p(x) = \frac{P_o(x)L(x)}{\sum P_o(x)L(x)} \tag{1}$$

$$L(x) = e^{-Q(x)} \tag{2}$$

where $p(x)$ is the posterior probability function, $P_o(x)$ is the prior probability function, and $L(x)$ is the likelihood function using $Q(x)$ as the objective function. The basis of this optimization method is the Bayesian type of minimization [40].
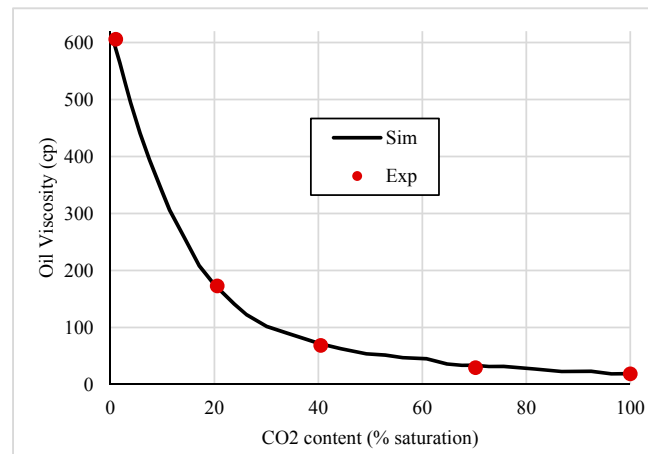

Figure 1. Experimental data (black dots) of oil viscosity versus CO_2 concentration as matched by the equation of states (EOS) model (black line).

For history matching, a tolerance limit of less than 1% of error was selected. It is also worth mentioning that different weight factors for each data point were assigned. The data points before breakthrough had a weight factor of zero because, before breakthrough, what is injected is produced and is not strongly dependent on relative permeability. This would enable more focusing on the matching of the curvatures after breakthrough. Also, if recorded data points were highly dense in some regions, a couple of points were chosen to have weight factor of 1 and the rest (in that region) were excluded. For instance, number of recorded data points of differential pressure (dP) in the in the early stages of the tests are highly dense, and they all have fairly similar values of dP. Therefore, two points of the existing 12 points were arbitrarily chosen with a weight factor of 1 and the rest (ten points of that region) had a weight factor of zero. This approach of "targeted history matching" would enable faster convergence of optimization.

The rationale for choosing 2D simulation over 3D is down to two main factors; firstly, the computation cost of each simulation, and secondly, our dimensionless analysis indicates that gravitational tongue would control the displacement pre-dominantly. For the computation time, adding another dimension in simulation (3D) would increase the run time exponentially. For 2D simulation, each run of the high resolution compositional model takes approximately a day, whereas (using eight CPUs of a desktop PC) a 3D model with the same gridding scheme (nx = 100, ny = 80, nz = 80) would take around a week using the same machine. It would therefore be impractical at this time to use 3D models for history matching of core scale experiments, which may require 1000 realizations of relative permeability.

Also, 3D models would be more representative for systems where viscous fingering dominates, which are best captured with more detailed 3D models. In the presence of an adverse mobility ratio and density contrast, the competition between the viscous and gravitational forces can bring about transitional behaviors between severe viscous fingering and a sharp gravitational tongue. To analyze the dominancy of the forces, Fayers extended Dietz theory [41] and proposed a dimensionless viscous-to-gravity parameter (NG) as expressed by Equation (3);

$$N_G = 2\left[\frac{\left(1 - \frac{\lambda_o}{\lambda_g}\right)q}{\lambda_o \Delta\rho g} - \theta\right] \times \left(\frac{H}{L}\right) \tag{3}$$

$N_G = 1$ can be regarded as the point where transition between gravity and viscous force becomes important, i.e., gravitational instabilities (tongue) are dominant below $N_G = 1$. Conversely, $N_G > 20$ has been reported as the region where viscous fingering is much stronger than gravitational tongue, which may occur if our coreflood experiments were performed in vertically oriented cores. Using the relevant parameters, CO_2 injection in horizontal results in $N_G \approx 0.05$, which is well below the threshold value of $N_G = 1$, and hence gravitational instabilities overtake the viscous fingering. This result implies that the injected CO_2 would override the resident oil, creating a tongue. In contrast with the uncertainty involved in the simulation of viscous fingering such as number of fingers and different behavior of each finger [42], formation of a gravitational tongue would mainly depend on the thickness of a single tongue and speed of its advancement. In other words, when the displacement is controlled by a sharp finger, 2D representation of the core would adequately capture the displacement patterns.

The procedure in Taura et al. [2] also suggested an empirical method for verifying the simulated in-situ saturation distribution for a case where an experimental saturation data is not available. This is important because relative permeability is a strong function of saturation distribution, and for a case with instability, infinite saturation paths are possible, and hence there is a need to verify the saturation distribution. Table 1 presents the experiments considered in the studies. Table 2 shows the basic properties of the core (Clashach sandstone) used in the experiments. The API gravity of the oil used in the experiment is 16. The experiments were performed at pressure of 1500 psig and 28 °C. Under these conditions, CO_2 is in a liquid state. This state of CO_2 would favor CO_2 dissolution into the oil, which would bring about significant reduction in oil viscosity. The injection rate was set at 7 cc/h, which is close to conventional reservoir advance rate of 1 ft/day. During the experiments, production of different fluids and differential pressure across the core were measured. Details of experimental procedure and information acquired from each experiment can be found in [43].

Table 1. Experiments used in the investigation of three-phase relative permeability.

Test ID	Test Description	Fluids	Core Orientation	Conditions
1	CO_2 injection into dead Crude-J	Injection fluid: CO_2 Resident oil: dead Crude-J Resident brine: 20,000 ppm	Horizontal	T = 28 °C, P = 1500 psig
2	Water injection into dead Crude-J	Injection fluid: brine Resident oil: dead Crude-J Resident brine: 20,000 ppm	Horizontal	T = 28 °C, P = 1500 psig
3	Tertiary water injection (after CO_2 injection)	Injection fluid: brine Initial oil: dead Crude-J Resident brine: 20,000 ppm	Horizontal	T = 28 °C, P = 1500 psig
4	Simultaneous water and CO_2 injection into dead Crude-J	Injection fluid: brine, CO_2 Resident oil: dead Crude-J Resident brine: 20,000 ppm	Horizontal	T = 28 °C, P = 1500 psig

Table 2. Core properties.

Core Properties	Value
Diameter (cm)	5.12
Length (cm)	32
Permeability to Brine (mD)	2500
Porosity (frac.)	0.2354
Swi (frac.)	0.126

3. Relative Permeability Correlation

Two different relative permeability functions were used to represent the two sets of two-phase flows. The gas/oil relative permeability was represented by a flexible three-parameter correlation known as the LET-type correlation [44]. This type of correlation was used due to its versatility in honoring the so-called "S-behavior" of gas relative permeability (Equations (4)–(6)). For water/oil

relative permeability, a simple power-law model (traditionally referred to as Corey correlations) was used (Equations (7) and (8)). Alternatively, the Stone II model [31] (Equation (9)) was chosen for the three-phase relative permeability correlation because of its simplicity and its bivariate nature, since the computed oil relative permeability depends on two saturation values: gas and water relative permeabilities. For history matching, the coreflood experiments, S_{gcrit}, S_{org}, L, E, T, K_{rg}, K_{rog} were considered for CO_2-oil relative permeability curves and S_{orw}, *no*, *nw*, K_{rw} were used for oil-water cases.

It should be noted that the objective of this work is not to examine the results of different three-phase oil relative models. The main focus of this work is to develop a methodology for estimating relative permeability based on displacement patterns in three-phase flow. Since the systems under study are heavily affected by viscous ratios and mass transfer, the objective is to demonstrate that, when two phase relative permeabilities are tuned based on a physical process taking place in one experiment (tertiary waterflood after CO_2 injection), the resultant *krs* can be used for another experiment with a similar displacement pattern (SWAG with CO_2). In other words, three-phase oil relative permeability models may affect the outcome of the simulations, but the tuned two-phase relative permeability would capture the flow behavior for the systems under study. Therefore, the approach is not purely predictive and is based on tuning the flow functions on one experiment to capture the displacement patterns, which would lead to an improved prediction of similar experiments.

$$S_{ge} = \frac{S_g - S_{gcrit}}{1 - S_{gcrit} - S_{org} - S_{wi}} \tag{4}$$

$$k_{rog} = K_{rog} \left(\frac{(1 - S_{ge})^{Lo}}{(1 - S_{ge})^{Lo} + Eo(S_{ge})^{To}} \right) \tag{5}$$

$$k_{rg} = K_{rg} \left(\frac{(S_{ge})^{Lg}}{(S_{ge})^{Lg} + Eg(1 - S_{ge})^{Tg}} \right) \tag{6}$$

$$k_{row} = K_{row} (S_{we})^{no} \tag{7}$$

$$k_{rw} = K_{rw} (1 - S_{we})^{nw} \tag{8}$$

$$K_{ro} = K_{rocw} \times \left\{ \left(\frac{K_{row}}{K_{rocw}} + K_{rw} \right) \left(\frac{K_{rog}}{K_{rocw}} + K_{rg} \right) - K_{rw} - K_{rg} \right\} \tag{9}$$

For capillary pressure information, there is one centrifuge experiment performed using an air-brine system on this core [45]. The air–brine capillary pressure can be modified for the systems used in this study, i.e., CO_2-oil and oil-water. Utilizing the famous Leverett formula [46], the capillary pressure of CO_2-oil and oil-water can be estimated;

$$P_{cow} = P_{caw} \times \frac{(\sigma \cos \theta)_{ow}}{(\sigma \cos \theta)_{aw}} \tag{10}$$

Provided that air–brine interfacial tension (IFT) is 72 dyne/cm and their contact angle is assumed to be zero, the capillary pressure of oil-water can be calculated with aid of measured IFT (i.e., 30.84 dyne/cm). It should be pointed that the contact angle of oil-water system using quartz substrate was measured and it was 25°. Since the core was not aged during the coreflood experiment, it would be fair assumption to use the measured contact angle for conversion of capillary pressure. For the CO_2–oil system, no measured value of IFT and contact angle was available. Hence, for converting the air-brine capillary pressure, the IFT of CO_2–oil was estimated using the tuned EOS, which was 1.33 dyne/cm. The CO_2–oil contact angle was assumed to be zero like air-brine system. In other words, CO_2–oil capillary pressure was obtained using the ratio of the CO_2–oil IFT to that of air-brine. Figure 2 depicts the estimated capillary pressure curves used in the process of history matching. CO_2 would not be miscible with the dead crude oil used in this study. As we reported the IFT between CO_2 and crude oil as 1.33 dyne/cm. CO_2 is partially dissolvable in the dead crude oil. After contacting CO_2 and

this crude oil, 82 cc CO_2 per cc of oil was dissolved in the oil, which indicates dissolution of CO_2 in the oil but not miscibility. Also, CO_2 was injected in vertical orientation (gravity stable CO_2 injection) and recovery factor was poor, which may indicate that CO_2 would not be miscible with this heavy oil [2]. Furthermore, it was demonstrated that same relative permeability curves can simulate vertical CO_2 injection and residual oil saturation to gravity-stable CO_2 injection would be 30%, which again indicates immiscibility of CO_2 and this crude oil [2].
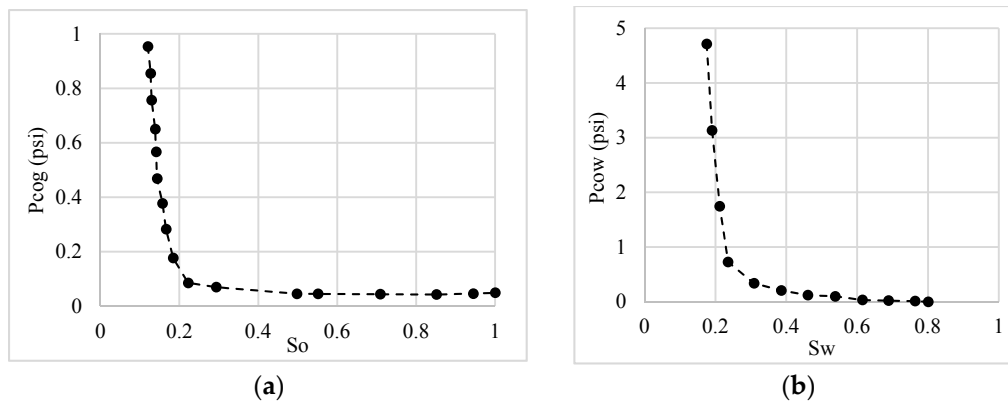
Figure 2. Capillary pressure curves for CO_2–oil (**a**) and oil-water (**b**) systems. The curves were estimated and corrected from a centrifuge experiment performed on the core with the air-brine system.

4. Estimation of Two-Phase Relative Permeability Curves

4.1. Secondary CO_2 Injection Experiment (CO_2/Oil Relative Permeability)

In this experiment, CO_2 was injected into heavy oil at a temperature and pressure of 28 °C and 1500 psi, respectively; the viscosity of pure CO_2 and crude oil at the experimental condition were 0.07 cp and 617 cp respectively. The injected CO_2 continuously dissolved in the oil and when it became fully saturated, the oil viscosity dropped drastically to 16 cp. Due to a highly unfavorable mobility ratio between CO_2 and viscous oil, the secondary CO_2 injection experiment is prone to frontal instabilities such as viscous fingering and gravity tonguing. Details of instability analysis can be found in Taura et al. [2]. For systems under frontal instabilities, a high-resolution 2D model that can effectively capture any instability in the displacement was therefore employed by conducting sensitivity analysis on the produced oil and the pressure at the inlet of the core. The optimum grid size required was determined as 100×80 grid (horizontal and vertical direction respectively). One issue pertinent to numerical simulation of displacements under frontal instability is the significance of numerical dispersions on the development of instabilities [47]. To address the impact of numerical dispersions, different simulation runs can be performed to sensitize the effect of grid size and gridding aspect ratio.

At large grid sizes, the front would become unrealistically averaged across the grid block, which may unphysically disperse the displacing fluid. On the other hand, when highly fine grids are used, the simulation run time would impose high computation costs. However, for this fundamental study, the effect of numerical dispersion should be minimized to obtain a representative set of relative permeability. To sensitize the impact of grid size, two systematic sensitivity analyses were carried out: (i) grid size in normal direction of injection and (ii) grid size aspect ratio, i.e., $\frac{\Delta x}{\Delta z}$ The importance of gridding aspect ratio has been highlighted where, for identical aspect ratios, the oil recovery for certain pore volume injected (PVinj) would follow a linear trend [42]. It can be postulated that as the grid size decreases at fixed aspect ratio, the oil recovery at breakthrough would exhibit a decreasing trend. Since the grid size would impact the breakthrough time (as demonstrated in our previous publications [2], in this sensitivity analysis on gridding, the basis for oil recovery was taken at 1 PVinj. Figure 3 shows the results of simulations performed for a different gridding scheme. As can be seen,

the simulation is highly affected by grid size. Also, for two aspect ratios sensitized, i.e., 2.51 and 5.02, linear trends on the oil recovery versus grid size can be identified, which indicates the unstable nature of the displacement. Furthermore, two linear trends would converge to a point where the oil recoveries at various aspect ratios would become identical. This point of convergence or interception point can be considered as the simulation with minimum impact of numerical dispersion. Therefore, as long as the simulation parameters (i.e., grid size and aspect ratio) are selected close to the interception point, the adversities related to numerical issues would be alleviated. However, there is another factor controlling the grid size, which is the run time of each simulation for history matching runs requiring hundreds of simulations. As highlighted in Figure 3, the difference in run time from a grid size of 0.16 cm (which corresponds to nx = 100) to the interception point is 30 h, which would only affect the oil recovery marginally. Therefore, the optimum gridding scheme as a suitable compromise between numerical dispersion and computation cost is 100 and 80 grids in injection (*x*) and normal to injection (*z*) directions, respectively.
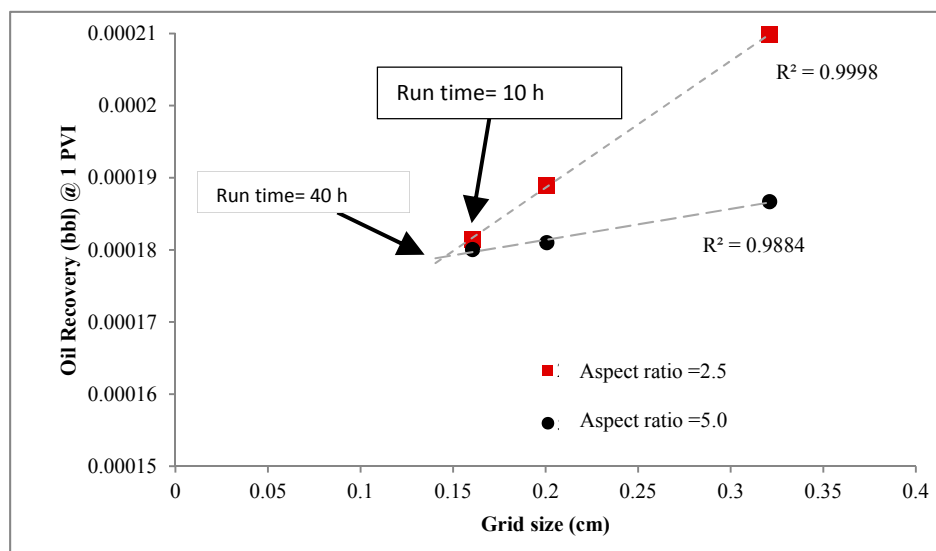

Figure 3. Sensitivity of grid size and gridding aspect ratio on the oil recovery (core test 1) to identify the suitable grid size for simulations to become minimally affected by numerical dispersion. Blue boxes highlight the run time for simulation with corresponding gridding.

Studies have also shown that capillary pressure (Pc) can exert significant influence on the stability of the front in such displacement. Sharma et al. [48] have shown that capillary forces can control interface movement in simulation results showing unfavorable displacement with viscous fingering. This can therefore significantly impact the saturation pattern and hence affect the estimated relative permeability. To illustrate this effect for the case of heavy oil displacement by CO_2, two sets of relative permeability curves were estimated by history matching; in the first case, the relative permeability curves were estimated including capillary pressure data while the second case had zero capillary pressure in the history matching. Figure 4 shows the result of the simulation of the history matched cumulative oil recovered and pressure at the inlet of the core. Figure 5 illustrates the two estimated relative permeability curves and it shows that in both cases, gas relative permeability has an *S*-shape characteristic while the oil relative permeability has exhibited less curvature, resembling a linear trend. However, including capillary pressure in the estimation has significantly affected the shape of the gas relative permeability.
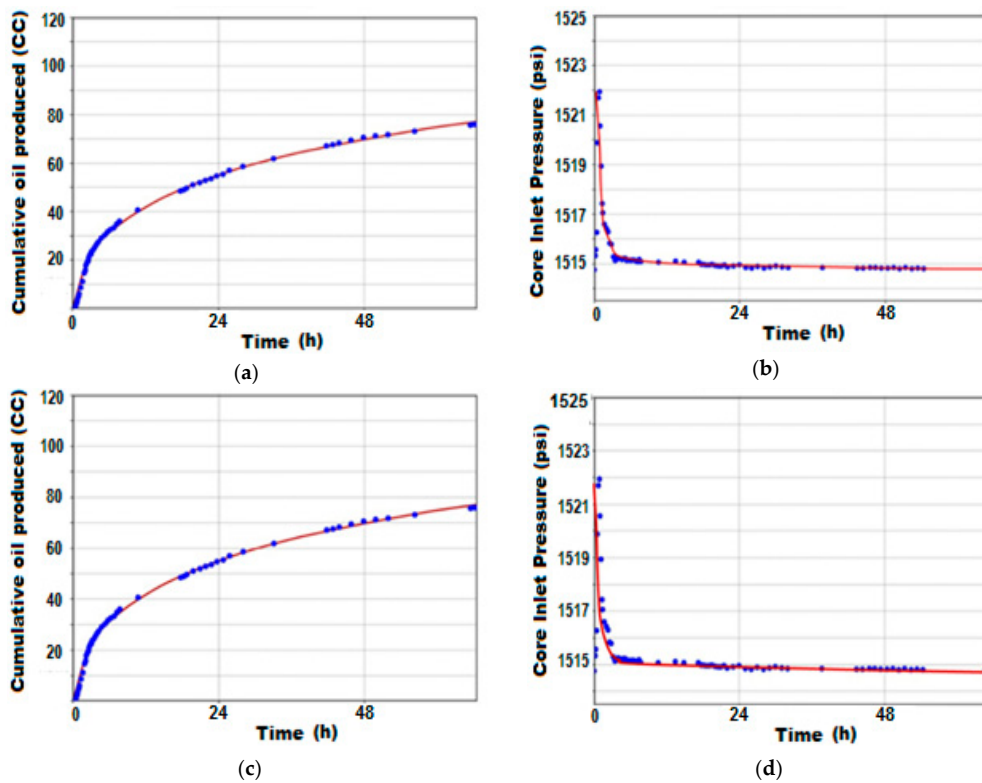
Figure 4. The results of the simulation of history matched oil recovered and the pressure at the inlet of the core for the two simulations of core test 1. Top figures (i.e., (**a**) for oil recovery and (**b**) for dP) are from estimation of relative permeability with capillary pressure while bottom figures ((i.e., (**c**) for oil recovery and (**d**) for dP) are from the case with zero capillary pressure (Pc). The red lines represent the results of history matching and the blue dots are experimental data.
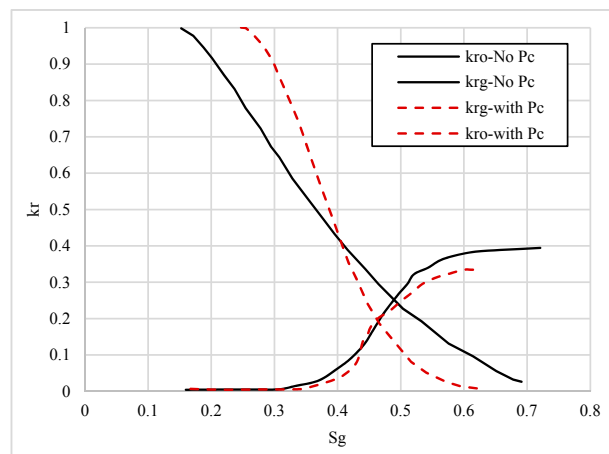

Figure 5. Tuned oil–gas relative permeability function for the two cases; with Pc (red dashed line) and without Pc (black line).

The implication of the change in shape of the relative permeability when Pc was included in the history matching process was manifested in the sweep pattern and the residual oil saturation, dictated by the end-point saturations in the relative permeability curves. In an unstable displacement, remaining oil saturation in the form of bypassed oil is mainly controlled by sweep efficiency. Figure 6 demonstrates the sweep patterns extracted from the simulations. It is obvious that, by including capillary pressure, the injected CO_2 has penetrated more efficiently close to the inlet, which could

change the estimated end-point saturations (i.e., S_{org}). In other words, the improved sweep efficiency resulted by inclusion of Pc was manifested in the change of end-points of relative permeability curves. It should be noted that end-point of the kr curves would express the pore-scale residual oil saturation and in a fixed oil recovery, the remaining oil would be split between residual oil and bypassed oil.
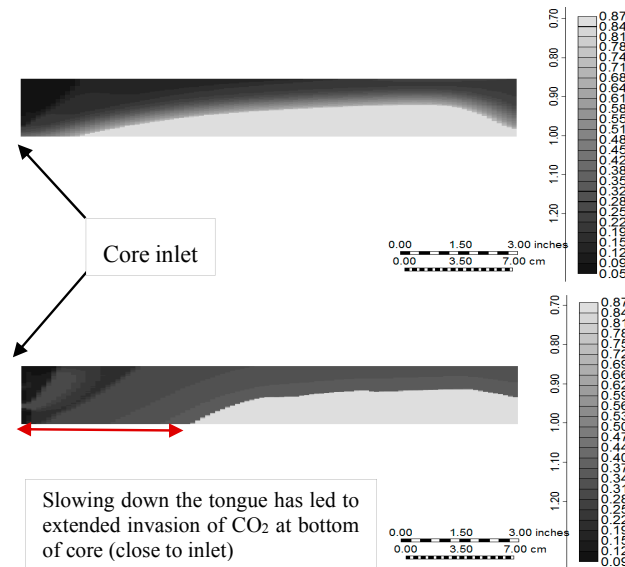

Figure 6. Oil saturation distribution (simulated for core test 1) at the end of CO_2 injection in two cases; no Pc (above image) with Pc (bottom image). The brighter the colour, the higher oil saturation exists in the grid block. Inclusion of capillary pressure, which would reduce frontal instability, has slowed down the onset of the gravity tongue and hence better sweep efficiency in the vicinity of core inlet.

It should also be pointed out that as LET functions [44] were employed, constructed kr curves can lead to slight jumps in the shapes of the curves, which would introduce numerical issues in the simulations at large scales. However, in simulations run during performed to tune relative permeability curves, the jumps in the shapes (as can be seen in red curve of Figure 5) did not introduce any numerical issue during history matching attempts.

4.2. Secondary Water Injection (Oil/Water Relative Permeability)

Similar to the secondary CO_2 injection, the oil/water relative permeability curves were estimated by history matching the waterflood experiment (Experiment 2) using two approaches: one with Pc included and the other with zero Pc. This was to determine the impact of Pc on frontal stability in the waterflood. Additionally, the history matching was conducted using a compositional simulator and with the same grid size (100×80) for consistency, even though no compositional effect and less instability was expected in the waterflood experiment. Figure 7 shows the results of the simulation of cumulative oil recovered and the differential pressure (as expressed in the form of inlet pressure) for the two cases; the top figures were from the case with Pc, while the bottom figures were from the case without Pc. Figure 8 compared the estimated relative permeability obtained from the history matching processes. Here, the inclusion of capillary pressure did not result in a dramatic change in the shape of the relative permeability curves and the two relative permeabilities are similar. However, a look at the saturation pattern in Figure 9 reveals an interesting effect of capillary pressure on frontal stability. Its inclusion has stabilized the front of the displacement (Figure 9 top) by dampening the viscous fingers otherwise developed when Pc was not included (bottom). This shows the significance of Pc on the control of interface movement in the displacement. It is important therefore to include an appropriate Pc curve in the numerical simulation to avoid misrepresenting the system.
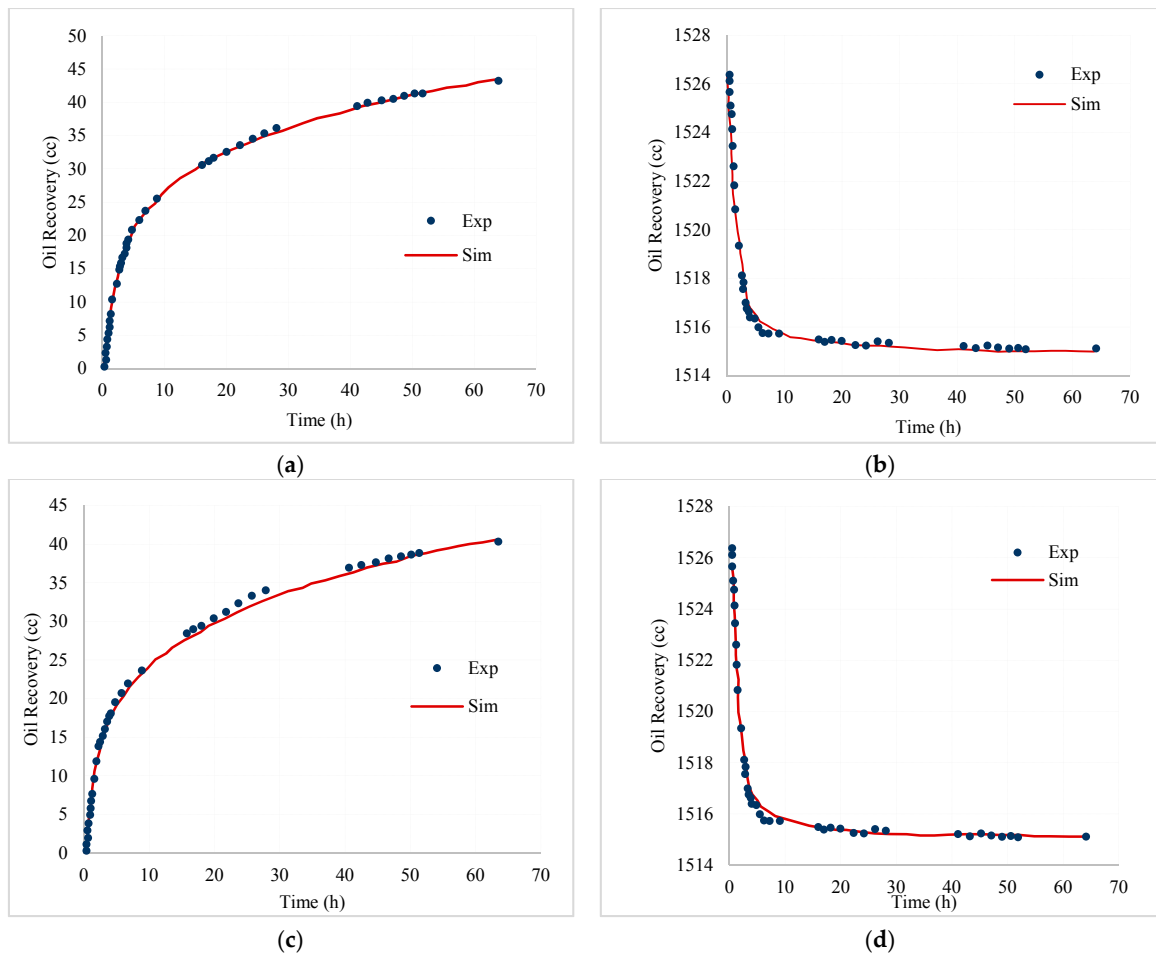
Figure 7. The results of history matched oil recovered and the pressure at the inlet of the core for the two simulations of core test 2 (water injection). Top figures (i.e., (**a**) for oil recovery and (**b**) for dP) are from estimation of relative permeability with capillary pressure while bottom figures ((i.e., (**c**) for oil recovery and (**d**) for dP) are from the case with zero Pc. The red lines represent the results of history matching and the blue dots are experimental data.
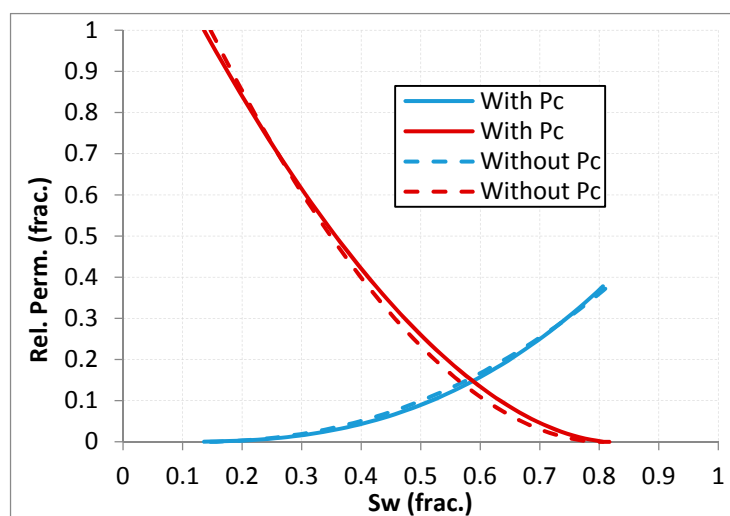

Figure 8. Tuned water-oil relative permeability curves estimated with two assumptions; with Pc (solid lines) and without Pc (dashed lines).
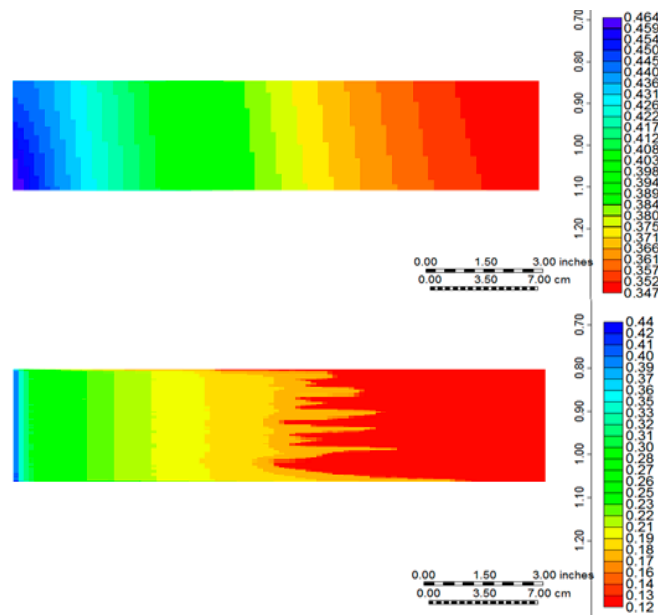
Figure 9. Simulation for core test 2. Comparison of simulation of the saturation pattern along the core for the two cases: with Pc in the history matching (**top**) and with zero Pc in the history-matching (**bottom**).

To estimate the two phase relative permeability curves, the 2D high resolution model was employed for both water and CO_2 injection cases. Profiles of saturation distribution extracted from simulation results have indicated that the oil displacement by water would be notably more stable than that of CO_2 injection. This set of experimental data has been previously simulated using one dimensional (1D) modelling [45] and the estimated relative permeabilities were given. Figure 10 illustrates the comparison between relative permeability curves obtained from 2D and 1D models. As can be seen, oil-water relative permeabilities are approximately similar in two cases. However, considerable differences can be observed between 1D and 2D models. This contrast in 1D and 2D models between oil-water and CO_2-oil relative permeabilities can be attributed to degree of instability identified from profiles of saturation distribution. Therefore, it is essential to use 2D models for the simulation of experiments involving CO_2 injection, such as tertiary water injection and CO_2-SWAG.
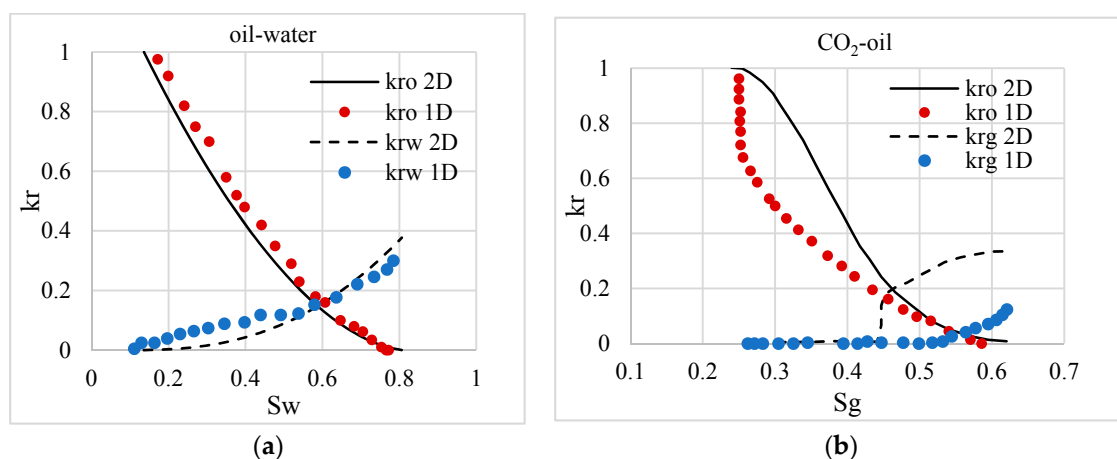

Figure 10. Comparison of relative permeabilities obtained from one and two dimensional modelling. Notable difference can be identified from oil–water cases (**a**) compared to CO_2–oil curves (**b**), which indicate the impact of frontal instability on the relative permeabilities.

5. Estimation of Three-Phase Gas/Oil/Water Relative Permeability from Tertiary Water Injection (Experiment 3)

The coreflood in Experiment 3 was conducted as a chase waterflood to the secondary CO_2 injection in Experiment 1 above. Unlike conventional WAG process in light oils, the chase waterflood in viscous oils would encounter two regions of remaining oil after CO_2 (gas) injection: (i) the residual oil due to capillarity (which is expressed in *Sorg*) in the swept area in which CO_2 dissolution occurred and has significantly reduced the oil viscosity and (ii) oil remained in bypassed regions whose oil still has the original viscosity value. Based on experimental findings acquired from several coreflood studies, water-alternating-CO_2 is potentially the most efficient cold displacement process compared to only water or CO_2 injections [6,49]. This is due to its benefiting from both better pore-scale and sweep efficiencies of CO_2 and water, respectively. Current knowledge of WAG modelling is based on the hysteresis formulations in which relative permeability functions of water/oil/gas are adjusted in successive injections of water and gas.

Therefore, because of the influential CO_2–oil interactions, there are several crucial factors in tertiary water injection that need to be taken care of in the simulation. These are listed as follows:

1. Viscosity and density of the oil in the swept region;
2. Viscosity and density of the bypassed oil;
3. Viscosity of the remaining CO_2 in the core at the end of the secondary CO_2 injection.

To estimate the three-phase relative permeability, LET and Corey correlations were used to represent gas/liquid and oil/water relative permeabilities, respectively, in the history matching process. The Stone II model, in which gas and water relative permeabilities can affect three phase oil relative permeabilities, was employed for the three-phase flow of gas, oil and water [31]. Having compositionally established the oil viscosities of swept and bypassed regions as 16 cp and 617 cp, respectively, the three-phase relative permeabilities were estimated. In this approach, the results of simulation of the secondary CO_2 injection (zero Pc case), i.e., distributions of fluids saturation and compositions in each grid block, which was history matched in Section 3 were used to initialize the model for tertiary water injection. Therefore, for history matching of water injection, the compositional variations in the core was considered to estimate oil viscosity in each grid block, which would produce the oil viscosity distribution between 16 cp and 617 cp depending on the amount of CO_2 dissolved in the oil. For the history matching runs, two dimensional optimizations were set up with compositional initialization of the model as described above.

Figure 11 demonstrates the simulation results in comparison with experimental data for oil recovered, gas produced, differential pressure and water production. The estimated tertiary relative permeability is shown in Figure 12. It can be observed that not only the end-point saturations were affected by tertiary water injection, but also the relative permeabilities changed. The changes (between secondary and tertiary injection scenarios) in oil/water relative permeability are much smaller compared to those of gas/liquid relative permeability. This can be due to the large variation in the viscosity ratios at the different cycles. For instance, in the secondary CO_2 injection, liquid CO_2 with a viscosity of 0.072 cp displaced the resident oil with a viscosity of 617 cp, whereas in the tertiary water injection, CO_2 in place with a viscosity of 0.8 cp (as estimated by a tuned equation of state) was displaced by water with a viscosity of 0.9 cp, which is more viscous than CO_2. Therefore, viscosity pairs are critical in the estimation of relative permeabilities, which in turn can be linked to the occurrence of frontal instabilities.
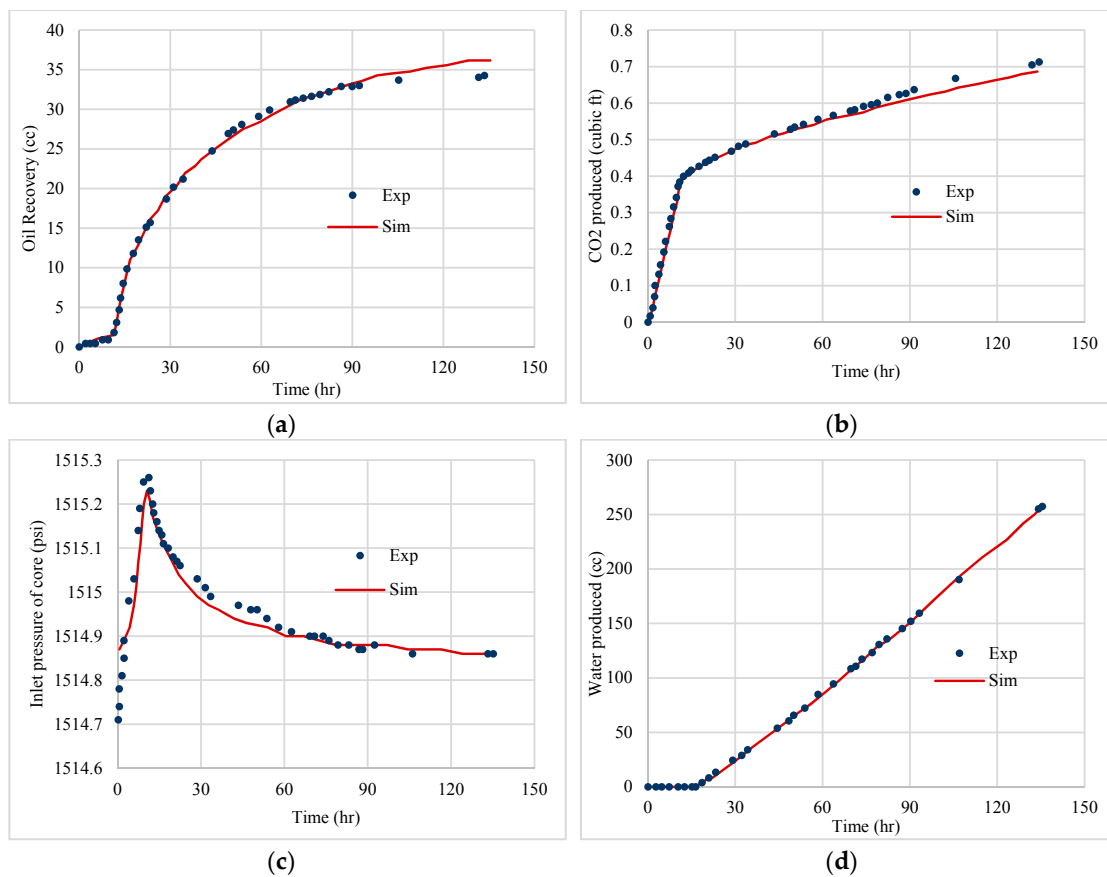
Figure 11. Simulation results for core test 3 obtained through history matching (red line) against the experimental information (blue dots) for (**a**) oil production, (**b**) gas (CO_2) production, (**c**) differential pressure across the core, and (**d**) water production.
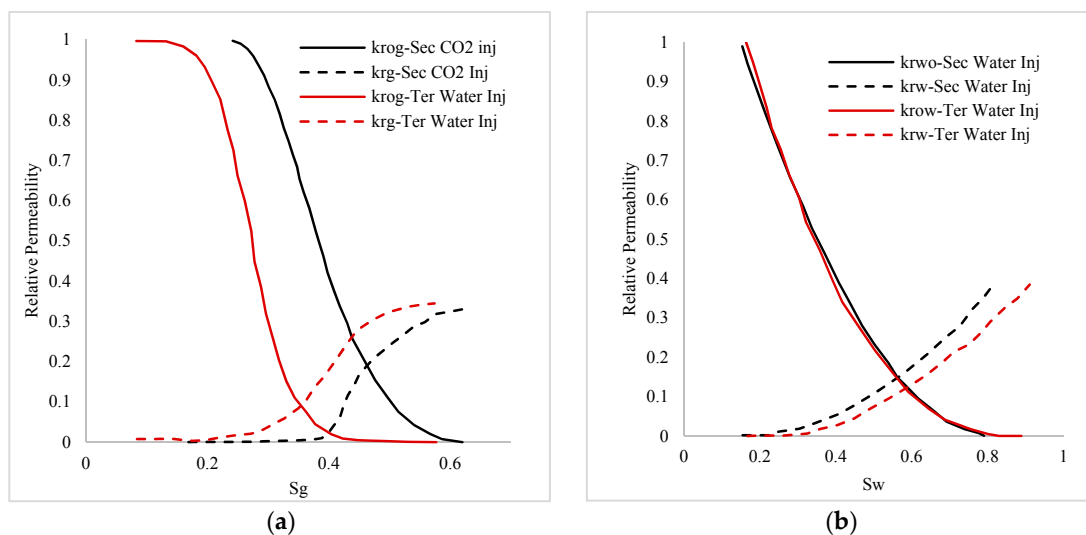

Figure 12. Water–oil (**b**) and oil–CO_2 (**a**) relative permeability obtained through history matching the corresponding coreflood experiments. The sequence of displacements, i.e., secondary or tertiary, can affect the relative permeability functions. In tertiary water injection, *Sorw* is notably lower than secondary water injection, which can attributed to improved viscosity of the oil after contacting with preceding injection (i.e., CO_2 injection).

In the case of the oil/water relative permeabilities, a notable change in end-point saturation can be identified, with only a slight change in the shape of relative permeabilities. In other words, the residual oil saturation in the waterflooding has been considerably improved. This improvement in end-point saturations can be attributed to a physical phenomenon, which is the better oil viscosity in the area previously swept by CO_2 (oil with viscosity of 16 cp due to CO_2 dissolution), which makes the oil more recoverable. Additionally, based on this simulation result, we can conclude that CO_2-WAG can perform efficiently in the case where CO_2 initially dissolves in the oil, reduces its viscosity, and is consequently followed by water injection, which then readily recovers more mobile oil.

The outcome of history matching performed for the tertiary water injection has exhibited a meaningful displacement efficiency that can be supported by the fact that the waterflood invasion would be controlled by the viscosity upgrading introduced by CO_2 dissolution. Figure 13 shows the water saturation distribution extracted from the simulation results, which highlights the sweeping pattern of the tertiary water advancement. In the early stage of water injection, water tended to underride the resident CO_2 and oil. However, the water-front became more stable when it encountered the bypassed oil at the bottom of the core with high viscosity (617 cp) as shown in the middle image. Later on, as the water advanced, the front flowed through the pre-swept area easier than the bypassed oil, which brought about another type of instability controlled by the contrast in viscosities of oil in two different regions. The main finding here was the preference of water to displace the resident gas compared to the residual oil in the bypassed region. In conventional WAG injection (light to medium oils), it is believed that water and gas would invade different paths based on the competition of capillary forces (or, in other words, wettability) [50]. Also, trapped gas saturation would contribute to oil recovery in water injection cycles by diverting the invading water to remaining oil saturations. However, as seen in the simulation of this experiment (post CO_2 injection in viscous oil systems), the large contrast in viscosities of displacing and displaced fluids would form a selection criterion for the water and gas paths. This process would have another implication: most of the hysteresis models have been derived based on the fluid trapping and wettability regimes, e.g. Land's [19] and Larsen and Skauge [51] models. However, here, the viscosity ratio would change both pore-scale and sweep efficiencies, which would necessitate a thorough investigation on the validity of hysteresis models in adverse mobility conditions.
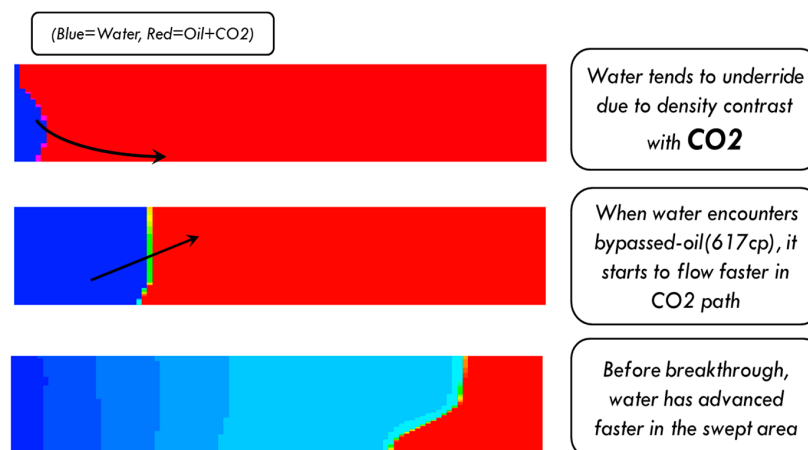

Figure 13. Simulated for core test 3, water saturation profile at different injection times indicating the preferred path by water resulting from the effect of preceding gas (CO_2) injection.

Simulations and history matching performed on two and three-phase displacements have indicated several findings. From the relative permeability curves estimated from high resolution history matching, it can be seen that tertiary waterflood would exhibit a lower residual oil saturation, which can be attributed to less viscosity of the resident oil after CO_2 injection. Therefore, it can be

postulated that changes in oil viscosity would outperform hysteresis effects in water-alternating- CO_2 injection scenarios for viscous oils. In simulations of WAG injection, employing WAG-hysteresis models would impose considerable computation cost and convergence issues. Hence, provided that hysteresis effects would not be dominant in viscous oils, excluding this option in the commercial simulators would facilitate simulation runs. However, this interpretation of the simulation results needs to be verified from experimental evidence. Emadi et al. performed a series of visualization experiments in which CO_2 and water injection scenarios had been investigated for a similar viscous oil [52]. Figure 14 depicts two snapshots of micromodel experiments where water injection was carried out after CO_2 injection, which is closely similar to the coreflood experiments analyzed in this simulation work. After CO_2 injection (Figure 14a), the remaining oil contacted with the CO_2 has a completely different color, which reflects lower viscosity of the oil due to CO_2 dissolution. When water was injected (Figure 14b), the invading water has demonstrated more efficiency to displace the oil with lower viscosity. This can be directly identified from comparison of pore-scale efficiencies at top (better displacement) and bottom (higher oil viscosity and poorer pore-scale efficiency) of the porous medium. Therefore, the interpretations from simulation results can be supported from micromodel observations.
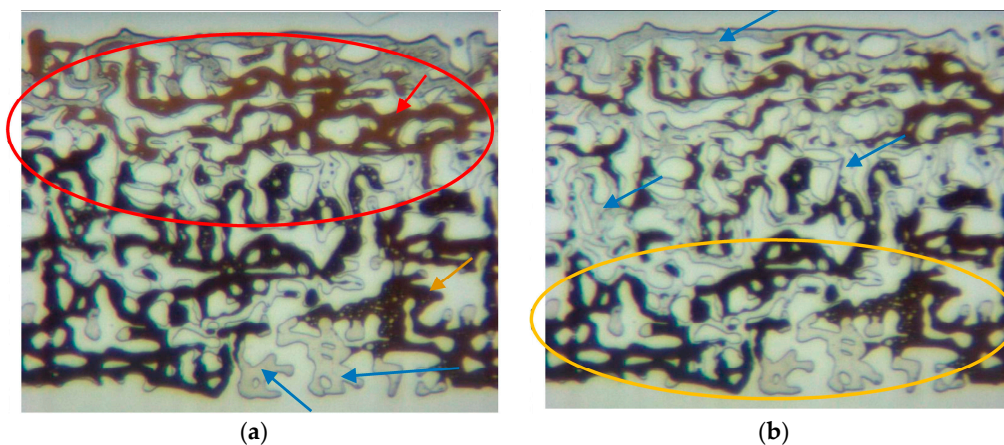

(a) (b)

Figure 14. Pore-scale observations obtained from Emadi et al. (2011) for before (**a**) and after (**b**) water injection. On the left hand side (**a**), a magnified section of micromodel is shown after CO_2 injection in which CO_2 could be dissolved into the oil at top section making the oil brighter (highlighted with red oval) and hence, less viscous. On the right hand side (**b**), waterflood after CO_2 injection could lead to more oil displacement in the areas (top sections) where CO_2 could be dissolved and make the oil more mobile. Also, the oil remained at the bottom (highlighted by yellow oval) could not be displaced by the invading water due to higher oil viscosity. These mechanisms could be successfully captured in simulation results. Red, yellow, and blue arrows point to the brighter oil contacted with CO_2, oil unaffected by CO_2, and water, respectively.

6. Simulation of Simultaneous Water and Gas Injection into Heavy Oil (Experiment 4)

In Experiment 4, water and CO_2 were simultaneously injected at equal rates (each one at 3.5 cc/h) in a process known as simultaneous water and gas (SWAG). In conventional light oil displacement using this method, capillary forces play a crucial part in the preference for pore occupancy by the fluids. However, in heavy oil displacement using SWAG, where the gas is partially dissolvable in the oil, which leads to a significant viscosity reduction, viscous forces are dominant over capillary forces in preference for pore occupancy by the fluids. Consequently, from flow functions point of view, a reliable set of relative permeability functions coupled with a consistent viscosity reduction correlation would suffice to simulate the coreflood experiments. Here, an attempt was made to perform a forward simulation (not history matching) where the SWAG coreflood experiment was simulated by using directly the relative permeability obtained in the previous history matching since the experimental condition (as well as the rock and fluid properties) are similar. Because CO_2 has a notably higher mobility compared

to water during the simultaneous injection, it is plausible that the injected CO_2 would move ahead of the water. This is also evident from the different breakthrough times of secondary CO_2 (Experiment 1) and water (Experiment 2) injections, where the breakthrough time of CO_2 was significantly earlier. In other words, it would be a reasonable assumption that CO_2 flow can be controlled by the relative permeabilities obtained from the secondary CO_2 injection process. However, two choices exist for the water relative permeability based on the water injection modes; either secondary or tertiary relative permeability. Therefore, two simulations were run in a 2D compositional model. Figure 15 shows the results of the simulation runs compared against the experimental data. The fluid production profiles highlighted that a reasonably good match can be achieved when a tertiary water-oil and secondary oil–CO_2 relative permeabilities were employed. The mean squared errors (expressed in percentage) for blue and red curves in Figure 15 are 5.15% and 19.88% respectively. However, it should be noted that the error of prediction by the blue curve is much lesser in first 40 h (1 PV injected) of the experiment, which is 1.56%.
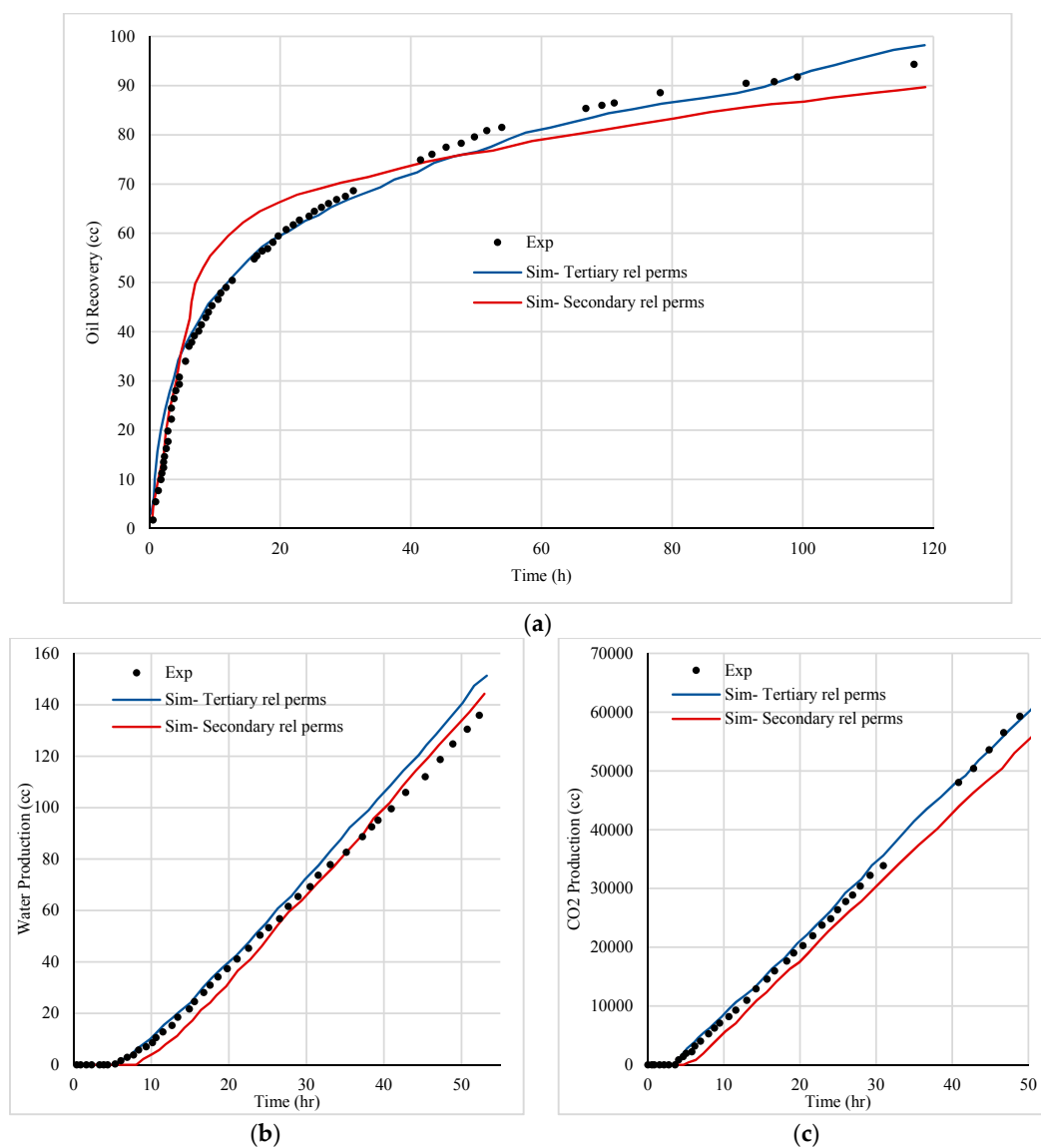

(**a**)

(**b**)

(**c**)

Figure 15. Simulated for core test 4, results of the fluid productions ((**a**) oil, (**b**) water, and (**c**) CO_2) obtained from simulation runs using secondary (red curves) and tertiary (blue curves) water–oil relative permeabilities. Comparison of simulation against experimental data (dots) indicating a better estimation for the case using tertiary water-oil relative permeability.

Although the simulations have not matched the experimental data perfectly, the mismatch is reasonably low and is acceptable for this highly complex system. In particular, the blue curve in Figure 15 (tertiary water–oil relative permeability case) has demonstrated an encouraging outcome in the early stages in which viscous forces were dominant. Figure 16 shows the result of simulation of the gas saturation distribution before the breakthrough, indicating the tendency of injected CO_2 to segregate gravitationally. This implies that CO_2 injection would be more efficient if injected in gravitationally stable scenarios. On the other hand, Figure 17 illustrates the pattern of water frontal advancement indicating that water initially flowed downward near the inlet in the early stage of the injection but later, it advanced upward and followed the CO_2 path because it had significantly lower resistance due to its oil having lower viscosity. Therefore, the efficiency of the SWAG displacement is mainly controlled by the extent of CO_2 invasion, which reduces the oil viscosity.
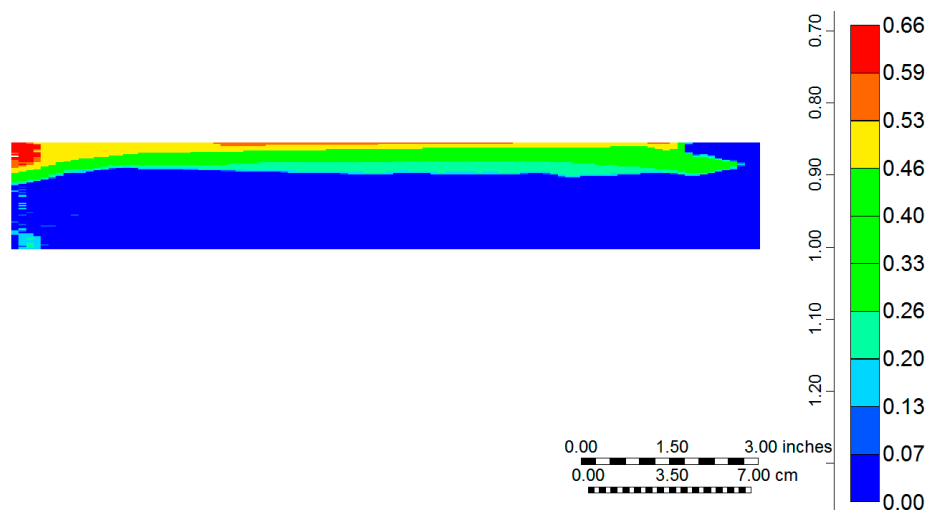

Figure 16. Simulated for core test 4, gas saturation distribution before CO_2 breakthrough indicating the CO_2 tendency to segregate.
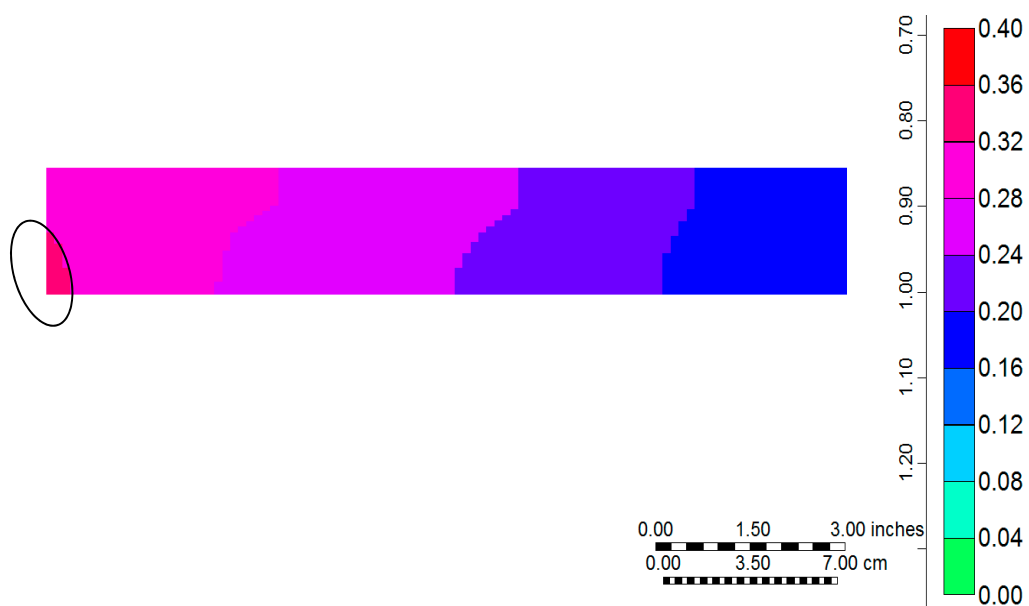

Figure 17. As obtained from simulation of core test 4, water saturation distribution at breakthrough of water. The accumulation of water highlighted with a black circle in the core inlet indicates the tendency of water to flow downwards.

Figure 18 shows the viscosity of the resident oil at two stages, namely the CO_2 breakthrough and the end of SWAG injection. The poor CO_2 sweep efficiency has resulted in leaving a relatively large volume of oil untouched (red area). Figure 19 also illustrates the oil saturation distribution at the end of the simulation; it shows a distinct characteristic of the displacement, which is that the residual oil saturation approached up to less than 5% at the top of the core where CO_2 and water flowed together, while the bottom of the core, which had only been partly swept by water, had relatively high residual oil saturation that is up to about 60 percent. Therefore, the SWAG type of CO_2 injection would efficiently reduce the oil saturation if CO_2 is injected in a gravity stable strategy.
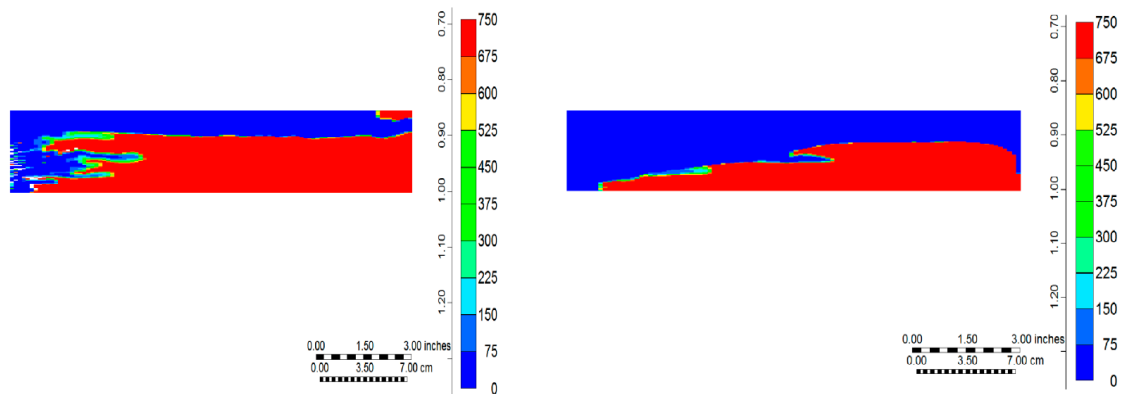

Figure 18. For simultaneous water and gas (SWAG) test (core test 4), the viscosity of the resident oil in the core at two simulation times: at CO_2 breakthrough (left image) and the end of the coreflood experiment (right image).
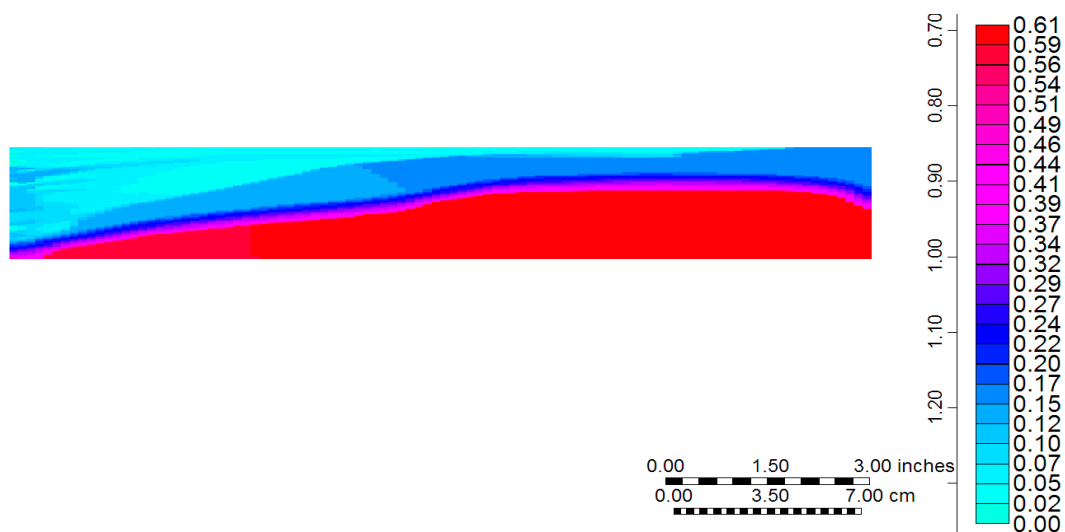

Figure 19. Oil saturation distribution throughout the core at the end of SWAG injection (core test 4), indicating very low residual oil saturation at the top of the core where CO_2 could invade and reduce the oil viscosity.

The improvements attained in the simulation of the SWAG experiment would indicate that the methodology proposed here for laboratory experiments (i.e., 2D high resolution models using a trained compositional simulator) would lead to obtain flow functions with predictive capabilities. As mentioned earlier in Section 4.2, this set of experimental data was used in another investigation using 1D modelling [45]. The outcome of that study demonstrated that, the relative permeability curves from 1D model would not be representative and cannot reproduce similar experiments. Also, it can be identified from that work that, for each particular experiment, history matching needs to be performed,

and hence different sets of relative permeabilities would be obtained. If water-alternating-CO_2 injection is to be implemented at large scales (e.g., field scales), different regions of reservoir would under different CO_2, water, and SWAG invasion types. When using these relative permeabilities at larger scales, it would not be feasible to use different relative permeabilities for different regions of the reservoir under different CO_2 and water flow behavior. Therefore, the new approach proposed in this work to estimate flow functions for systems under very complex processes would lead to a set of relative permeabilities that would enable a capturing mechanism and reproduce similar experiments, which may make them suitable for large scale simulations.

7. Summary and Conclusions

An improved methodology was developed to simulate three-phase flow in core scales where significant mass transfer and frontal instability existed. Secondary and tertiary oil/water relative permeability was estimated by history matching the experiment in which water was used to chase a CO_2 flood. The following conclusions were drawn from the simulations performed on the coreflood experiments:

The simulation of the tertiary water injection shows that water preferred to follow the path already opened by the previously-injected CO_2. However, this mechanism is different from the conventional water alternating gas Injection (WAG), where water is expected to open up a new path different from that of the gas. Here, the water prefers to follow the path of the CO_2 because the dissolution of the gas in the oil has significantly reduced the viscosity of the trapped oil in the path of the CO_2. Hence, the lower resistance in the CO_2 path compared to that in the bypassed oil makes it more preferable for the tertiary water to follow.

Two simulation runs were performed to reproduce a three-phase flow experiment in which CO_2 and water were injected simultaneously (SWAG). The results showed that the experimental fluid production data could be adequately matched using the secondary gas–oil and tertiary water–oil relative permeability curves. This can be explained by the notably higher tendency of CO_2 to flow ahead of water, creating a situation where the secondary CO_2 injection was replicated with the injected water chasing the CO_2. It could be concluded the conventional hysteresis analyses applicable to light oils cannot be utilized for viscous oils, since the flow characteristics are mainly controlled by viscosity variations. Therefore, a simulation model well-defined on an unstable system (high-resolution 2D model with tuned EOS) would be able to predict different scenarios of CO_2 and water injection where significant mass transfer can bring about effective viscosity reductions. It should be pointed out that this work did not focus on the performance of three-phase relative permeability function (such as Stone I, Stone II, Baker, and etc.), which may affect the results. Herein, the improved methodology has been proposed to model WAG scenarios in heavy oil displacements based on the physics of CO_2 and water preferential paths.

Author Contributions: Pedram Mahzari: Designed and performed the research and wrote the manuscript. Usman Taura: Performed the research and wrote the manuscript. Alexander J. Cooke: Wrote the manuscript. Mehran Sohrabi: Designed the research and wrote the manuscript.

Conflicts of Interest: The authors declare no conflict of interest.

Nomenclature

S_{ge}	Effective gas saturation
S_g	Gas saturation
S_{gcrit}	Critical gas saturation above which gas starts to flow
S_{org}	Residual oil saturation after gas flood
S_{wi}	Initial water saturation
K_{rog}	Oil relative permeability in gas table
K_{rg}	Gas relative permeability
K_{ro}	Endpoint oil rel. perm. (max krog)
K_{rg}	Endpoint gas rel. perm. (max krg)
$L_{o,g}$	Exponent for lower part of kro and krg
$E_{o,g}$	Coefficient for the elevation of kro and krg
$T_{o,g}$	Exponent for top part of kro and krg
k_{row}	Oil relative permeability (in water table)
K_{row}	End-point oil relative permeability (max krow)
S_{we}	Effective water saturation
n_o	Corey exponent for oil relative permeability
n_w	Corey exponent for water relative permeability
q	Superficial velocity (flow rate per unit of area), m/s
$\Delta\rho$	Density difference, kg/m^3
θ	Degree of inclination of core
λ	Mobility (permeability divided by viscosity)
H	Core thickness, m
L	Core length, m

References

1. Sherwood, J.D. Unstable fronts in a porous medium. *J. Comput. Phys.* **1987**, *68*, 485–500. [CrossRef]
2. Taura, U.; Mahzari, P.; Sohrabi, M.; Farzaneh, S.A. A New Methodology for Improved Estimation of Two-Phase Relative Permeability Functions for Heavy Oil Displacement Involving Compositional Effects and Instability. In Proceedings of the SPE International Heavy Oil Conference and Exhibition, Mangaf, Kuwait, 6–8 December 2016.
3. Sankur, V.; Emmanuel, A.S. A Laboratory Study of Heavy Oil Recovery with CO_2 Injection. In Proceedings of the 1983 California Regional Meeting, Ventura, CA, USA, 23–25 March 1983.
4. Araktingi, U.G.; Orr, F.M., Jr. Viscous Fingering in Heterogeneous Porous Media. *SPE Adv. Technol. Ser.* **1993**, *1*, 71–80. [CrossRef]
5. Cuthiel, D.; Kissel, G.; Jackson, C.; Frauenfeld, T.; Fisher, D.; Rispler, K. Viscous Fingering Effects in Solvent Displacement of Heavy Oil. *J. Can. Pet. Technol.* **2006**, *45*, 29–39. [CrossRef]
6. Emadi, A. Mechanistic Study of Improved Heavy Oil Recovery by CO_2-Foam Injection. In Proceedings of the SPE Enhanced Oil Recovery Conference, Kuala Lumpur, Malaysia, 19–21 July 2011.
7. Sohrabi, M.; Emadi, A. Novel Insights into the Pore-Scale Mechanisms of Enhanced Oil Recovery by CO_2 Injection. In Proceedings of the EAGE Annual Conference and Exhibition Incorporating SPE Europec, Copenhagen, Denmark, 4–7 June 2012.
8. Garcia, F.M. A Successful Gas-Injection Project in a Heavy Oil Reservoir. In Proceedings of the 58th Annual Technical Conference and Exhibition, San Francisco, CA, USA, 5–8 October 1983.
9. Mai, A.; Bryan, J.; Goodarzi, N.; Kantzas, A. Insights into Non-Thermal Recovery of Heavy Oil. *J. Can. Pet. Technol.* **2009**, *48*, 27–35. [CrossRef]
10. Outmans, H.D. Nonlinear theory for frontal stability and viscous fingering in porous media. *Soc. Pet. Eng. J.* **1962**, *2*, 165–176. [CrossRef]
11. Peters, E.J.; Flock, D.L. The Onset of Instability during Two-Phase Immiscible Displacement in Porous Media. *SPE J.* **1981**, *21*, 249–258. [CrossRef]

12. Jerauld, G.R.; Nitsche, L.C.; Teletzke, G.F.; Davis, H.T.; Scriven, L.E. Frontal Structure and Stability in Immiscible Displacement. In Proceedings of the SPE Enhanced Oil Recovery Symposium, Tulsa, OK, USA, 15–18 April 1984.

13. Kueper, B.H.; Frind, E.O. An overview of immiscible fingering in porous media. *J. Contam. Hydrol.* **1988**, *2*, 95–110. [CrossRef]

14. Jerauld, G.R.; Salter, S.J. The effect of pore-structure on hysteresis in relative permeability and capillary pressure: Pore-level modelling. *Transp. Porous Media* **1990**, *5*, 103–151. [CrossRef]

15. Riaz, A.; Tchelepi, H.A. Linear stability analysis of immiscible two-phase flow in porous media with capillary dispersion and density variation. *Phys. Fluids* **2004**, *16*, 4727–4737. [CrossRef]

16. Boukadi, F.H.; Bemani, A.S.; Babadagli, T. Investigating Uncertainties in Relative Permeability Measurements. *Energy Sources* **2005**, *27*, 719–728. [CrossRef]

17. Kokal, S.; Maini, B.B. An Improved Model For Estimating Three-Phase Oil-Water-Gas Relative Permeabilities From Two-Phase Oil-Water And Oil-Gas Data. *J. Can. Pet. Technol.* **1990**, *29*, 105–113. [CrossRef]

18. Muqeem, M.A.; Bentsen, R.G.; Maini, B.B. An Improved Steady-State Technique for Three-Phase Relative Permeability Measurements. In Proceedings of the Annual Technical Meeting, Calgary, AB, Canada, 9–12 May 1993.

19. Land, C.S. Calculation of Imbibition Relative Permeability for Two- and Three-Phase Flow from Rock Properties. *SPE J.* **1968**, *8*, 149–156. [CrossRef]

20. Akhlaginia, M.; Torabi, F.; Chan, C.W. Estimation of Three-Phase Relative Permeability Isoperms in Heavy Oil/Water/Carbon Dioxide and Heavy Oil/Water/Methane Systems. In Proceedings of the SPE Heavy Oil Conference Canada, Calgary, AB, Canada, 11–13 June 2013.

21. Honarpour, M.M.; Koederitz, F.; Herbert, A. *Relative Permeability of Petroleum Reservoirs*; CRC Press Inc.: Boca Raton, FL, USA, 1986.

22. Welge, H.J. Displacement of Oil from Porous Media by Water or Gas. *Trans. AIME* **1949**, *179*, 133–145. [CrossRef]

23. Johnson, E.F.; Bossler, D.P.; Naumann, V.O. Calculation of Relative Permeability from Displacement Experiments. *Pet. Trans. AIME* **1959**, *216*, 370–372.

24. Jones, S.C.; Roszelle, W.O. Graphical Techniques for Determining Relative Permeability from Displacement Experiments. *J. Pet. Technol.* **1978**, *30*, 807–817. [CrossRef]

25. Jennings, J.W.; Mcgregor, D.S., Jr.; Morse, R.A. Simultaneous Determination of Capillary Pressure and Relative Permeability by Automatic History Matching. *SPE Form. Eval.* **1988**, *3*, 322–328. [CrossRef]

26. Li, H.; Chen, S.; Yang, D.; Tontiwachwuthikul, P. Estimation of Relative Permeability by Assisted History Matching Using the Ensemble Karlman Filter Method. In Proceedings of the Canadian International Petroleum Conference, Calgary, AB, Canada, 16–18 June 2009.

27. Zhang, Y.; Song, C.; Zheng, S.; Yang, D. Simultaneous Estimation of Relative Permeability and Capillary Pressure for Tight Formations from Displacement Experiments. In Proceedings of the SPE Canadian Unconventional Resources Conference, Calgary, AB, Canada, 30 October–1 November 2012.

28. Chardaire-Riviere, C.; Chavent, G.; Jaffre, J.; Jun, L. Multiscale Representation for Simultaneous Estimation of Relative Permeabilities and Capillary Pressure. In Proceedings of the 65th Annual Technical Conference and Exhibition, New Orleans, LA, USA, 23–26 September 1990.

29. Chardaire-Riviere, C.; Chavent, G.; Jaffre, J.; Liu, J.; Bourbiaux, B.J. Simultaneous Estimation of Relative Permeabilities and Capillary Pressure. *SPE Form. Eval.* **1992**, *7*, 283–289. [CrossRef]

30. Stone, H.L. Probability Model for Estimating Three-Phase Relative Permeability. *J. Pet. Technol.* **1970**, *22*, 214–218. [CrossRef]

31. Stone, H.L. Estimation of Three-Phase Relative Permeability and Residual Oil Data. *J. Can. Pet. Technol.* **1973**, *12*, 54–61. [CrossRef]

32. Baker, L.E. Three-Phase Relative Permeability Correlations. In Proceedings of the SPE/DOE Enhanced Oil Recovery Symposium, Tulsa, OK, USA, 16–21 April 1988.

33. Carlson, F.M. Simulation of relative permeability hysteresis to the non-wetting phase. In Proceedings of the 56th Annual Fall Technical Conference and Exhibition of the SPE of AIME, San Antonio, TX, USA, 5–7 October 1981.

34. Braun, E.M.; Holland, R.F. Relative permeability hysteresis: Laboratory measurements and a conceptual model. *SPE Reserv. Eng.* **1995**, *10*, 222–228. [CrossRef]

35. Spiteri, E.J.; Juanes, R.; Blunt, M.J.; Orr, F.M. A new model of trapping and relative permeability hysteresis for all wettability characteristics. *SPE J.* **2008**, *13*, 277–288. [CrossRef]

36. Beygi, M.R.; Delshad, M.; Pudugramam, V.S.; Pope, G.A.; Wheeler, M.F. Novel Three-Phase Compositional Relative Permeability and Three-Phase Hysteresis Models. *SPE J.* **2015**, *20*, 21–34. [CrossRef]

37. Jerauld, G.R. General three-phase relative permeability model for Prudhoe Bay. *SPE Reserv. Eng.* **1997**, *12*, 255–263. [CrossRef]

38. Blunt, M.J. An Empirical Model for Three-Phase Relative Permeability. *SPE J.* **2000**, *5*, 435–445. [CrossRef]

39. Al-Dhahli, A.R.; Geiger, S.; van Dijke, M. Three-Phase Pore-Network Modeling for Reservoir with Arbitrary Wettability. *SPE J.* **2012**, *18*, 285–295. [CrossRef]

40. Computer Modeling Group Ltd. *CMOST User's Guide*, version 2009.10; Computer Modeling Group Ltd.: Calgary, AB, Canada, 2009.

41. Fayers, J.; Muggeridge, A. Extensions to Dietz theory and behaviour of gravity tongues in slightly tilted reservoirs. *SPE Reserv. Eng.* **1990**, *5*, 487–494. [CrossRef]

42. Christie, M.A.; Jones, A.D.W.; Muggridge, A.H. Comparison between Laboratory Experiments and Detailed Simulations of Unstable Miscible Displacement Influenced by Gravity. In *North Sea Oil and Gas Reservoirs—II*; Norwegian Institute of Technology (NTH): Trondheim, Norway, 1990; pp. 245–250.

43. Farzaneh, S.A.; Sohrabi, M.; Emadi, A. Experimental Investigation of CO_2, CO_2SWAG, and CO_2-Foam Injection Scenarios for Enhanced Heavy Oil Recovery. In Proceedings of the 18th European Symposium on Improved Oil Recovery, Dresden, Germany, 14–16 April 2015.

44. Lomeland, F.; Ebeltoft, E.; Thomas, W.K. A New Versatile Relative Permeability Correlation. In Proceedings of the International Symposium of the Society of Core Analysts, Toronto, ON, Canada, 21–25 August 2005.

45. Olufemi, W.S.; Sohrabi, M.; Shaverdi, H. Are Existing Three Phase Relative Permeability Models Adequate in Modeling Heavy Oil WAG Processes? In Proceedings of the SPE Heavy Oil Conference-Canada, Calgary, AB, Canada, 10–12 June 2014.

46. Leverett, M.C. Capillary Behavior in Porous Solids. *Trans. AIME* **1941**, *142*, 152–169. [CrossRef]

47. Lantz, R.B. Quantitative Evaluation of Numerical Diffusion (Truncation Error). *Soc. Pet. Eng. J.* **1971**, *11*, 315–320. [CrossRef]

48. Sharma, J.; Inwood, S.B.; Kovscek, A. Experiments and Analysis of Multiscale Viscous Fingering during Forced Imbibition. *SPE J.* **2012**, *17*, 1142–1159. [CrossRef]

49. Lim, G.B.; Kry, P.R.; Lebel, J.P.; Kwan, M.Y. Cyclic Solvent Process for In-Situ Bitumen and Heavy Oil Production. U.S. Patent 6769486-B2, 3 August 2004.

50. Mahzari, P.; Sohrabi, M. An Improved Approach for Estimation of Flow and Hysteresis Parameters Applicable to WAG Experiments. *Fuel* **2017**, *197*, 359–372.

51. Larsen, J.A.; Skauge, A. Methodology for numerical simulation with cycle-dependent relative permeabilities. *SPE J.* **1998**, *3*, 163–173. [CrossRef]

52. Emadi, A.; Sohrabi, M.; Jamiolahmady, M.; Ireland, S.; Robertson, G. Reducing heavy oil carbon footprint and enhancing production through CO_2 injection. *Chem. Eng. Res. Des.* **2011**, *89*, 1783–1793. [CrossRef]